

Numerical Resolution of CO₂ Transport Dynamics

Alexandre Morin* Peder K. Aursand† Tore Flåtten† Svend T. Munkejord†

Abstract

We consider a hyperbolic system of conservation laws describing multicomponent flows through a transport pipeline, with applications to CO₂ transport and storage. We demonstrate that numerical dissipation easily leads to an underestimation of the amplitude of pressure pulses and the resulting pipe strain. We argue that recently developed high-resolution methods, particularly adapted to our current model, are essential tools for an accurate operations analysis.

1 Introduction

An important factor in carbon dioxide (CO₂) capture and storage (CCS) is the transport between the point of capture and the point of storage. A main focus of the newly established BIGCCS centre [2], a consortium consisting of international universities, research institutions and industry partners, is the development of coupled fluid-mechanical and thermodynamic models with material science models to simulate crack propagation in CO₂ pipelines.

Such pipe flow will take place at high pressures, where the CO₂ is in a supercritical (liquid-like) state. Due to failure, or planned maintenance, the pipe can be depressurized, leading to cooling. If the temperature becomes low enough, the pipe material may become brittle, causing a rupture and much damage. Therefore, for a proper pipeline design, it is necessary to be able to estimate the pipe cooling during depressurization.

This requires the formulation of adequate thermodynamic and fluid-mechanical models, and an accurate numerical solution of these models. Hence potential errors in the operations analysis may arise from two separate sources:

- *Modelling errors*, i.e. failure of the underlying mathematical models to correctly capture physical reality;

- *Numerical errors*, i.e. failure of the chosen numerical method to represent the correct solution of the mathematical problem to a satisfactory degree of accuracy.

The models of interest typically take the form of systems of hyperbolic partial differential equations [9]. It is well known in the scientific community that artificial diffusion, needed to stabilize the numerical solution, may lead to severe loss of accuracy [7].

With this paper, we wish to increase awareness towards the fact that even a highly accurate *mathematical* model may produce untrustworthy results if proper *numerical* methods are not employed for industrial simulations. To this end, we compare an *upwind high-resolution* scheme with a *central first-order* scheme, namely the MUSTA scheme previously investigated for the current model in [9].

Our upwind scheme will be based on the approximate Riemann solver of Roe [10], and high resolution will be obtained by the *wave-limiter* approach of LeVeque [7].

In order to construct our Roe scheme, we must overcome the difficulty that our thermodynamic state relations are generally highly complex. They may consist of a combination of analytical state equations, mixing rules, and tabular interpolations. For all practical purposes, we must be able to treat our interface to thermodynamics as a black box.

In situations like these, *fully numerical* Roe schemes are often applied [12]. However, for reasons of simplicity and efficiency, we wish to consider a more analytical strategy where the Roe matrix involves only *partially numerical* constructions. To this end, we will largely follow the approach of Abgrall [1], and use an idea suggested by Glaister [6] for incorporating a general pressure function into our Roe scheme.

Our paper is organized as follows: In Section 2, we describe the governing equations of our multicomponent model. In Section 2.1, we discuss in some detail the particular thermodynamic submodels chosen for the purposes of this paper. In Section 2.2.1, we analytically derive the velocities and composition of the various waves associated with the model.

In Section 3, we derive our Roe solver. In Section 3.2.2 we describe more precisely how we are able to

*Dept. of Energy and Process Engineering, Norwegian University of Science and Technology (NTNU), NO-7491 Trondheim, Norway

†SINTEF Energy Research, NO-7465 Trondheim, Norway.
Email: Alexandre.Morin@sintef.no, pederka@stud.ntnu.no, Tore.Flatten@sintef.no, Svend.T.Munkejord@sintef.no.

incorporate a general black-box pressure function into the scheme in a smooth manner.

In Section 4, we present some numerical simulations, where we compare our high-resolution Roe scheme to a MUSTA scheme. In Sections 4.1–4.2, we focus on a couple of *shock tube* problems in order to illustrate the behaviour of the schemes on the individual waves. In Section 4.3, we present a case more relevant for industrial applications, where we study the effect of depressurization of a pipe.

Finally, our work is summarized in Section 5.

2 The Model

We consider flows of N different chemical species (components) along a transport pipeline. The model we will be studying assumes that the flow variables are averaged over the pipe cross section. Hence spatial dependence is only along the x -axis, and we obtain a system of conservation laws in the form

$$(2.1) \quad \frac{\partial \mathbf{U}}{\partial t} + \frac{\partial \mathbf{F}(\mathbf{U})}{\partial x} = \mathbf{Q}(\mathbf{U}),$$

to be solved for the unknown vector \mathbf{U} . Here \mathbf{U} is the vector of conserved variables, \mathbf{F} is the vector of fluxes, and \mathbf{Q} is the vector of sources.

Our model is similar to the one studied by Abgrall [1]. It consists of $N + 2$ separate conservation equations; one for the masses of each component, as well as conservation equations for the total momentum and energy of the mixture. More precisely, we have

- *Conservation of mass:*

$$(2.2) \quad \frac{\partial m_i}{\partial t} + \frac{\partial}{\partial x} (m_i v) = 0 \quad \forall i \in \{1, \dots, N\},$$

- *Conservation of momentum:*

$$(2.3) \quad \frac{\partial \rho v}{\partial t} + \frac{\partial}{\partial x} (\rho v^2 + p) = Q_v,$$

- *Conservation of energy:*

$$(2.4) \quad \frac{\partial E}{\partial t} + \frac{\partial}{\partial x} (v(E + p)) = Q_e.$$

Herein, the nomenclature is as follows:

m_i	- partial density of component i	kg/m^3 ,
ρ	- density of the mixture	kg/m^3 ,
v	- velocity of the mixture	m/s ,
p	- common pressure	Pa ,
e_i	- internal energy of component i	m^2/s^2 ,
E	- total energy of the mixture	$\text{kg}/(\text{m}\cdot\text{s}^2)$,
Q_v	- momentum source terms	$\text{kg}/(\text{m}^2\cdot\text{s}^2)$,
Q_e	- energy source terms	$\text{kg}/(\text{m}\cdot\text{s}^3)$.

Furthermore, the following relations hold:

$$(2.5) \quad \rho = \sum_{i=1}^N m_i,$$

$$(2.6) \quad E = \frac{1}{2} \rho v^2 + \sum_{i=1}^N m_i e_i.$$

2.1 Thermodynamic Relations. An essential feature of the numerical methods presented in this paper is that they are straightforwardly applicable to an arbitrary thermodynamic description of the mixture, including the possibility of phase transitions for each component. Hence, we will generally assume only that the mixture is at all times in thermodynamic equilibrium, and that there exists state relations

$$(2.7) \quad p = p(\epsilon, m_1, \dots, m_N),$$

$$(2.8) \quad T = T(\epsilon, m_2, \dots, m_N)$$

for the pressure and temperature of the mixture. Herein,

$$(2.9) \quad \epsilon = \sum_{i=1}^N m_i e_i.$$

However, in order to present reproducible results, the thermodynamics used for the simulations of this paper will be based on two simplifying assumptions:

1. The components are assumed to be immiscible;
2. Each component follows a *stiffened gas* equation of state, as described by Menikoff [8].

Note that none of these simplifying assumptions are required to derive the numerical solver.

The assumption of immiscibility implies that each component follows separate pressure and temperature laws:

$$(2.10) \quad p = p(\rho_i, e_i) \quad \forall i,$$

$$(2.11) \quad T = T(\rho_i, e_i) \quad \forall i,$$

where ρ_i is the density of component i . The stiffened gas EOS is fully defined by its *Helmholtz free energy*:

$$(2.12) \quad A(\rho, T) = c_v T (1 - \ln(T/T_0)) + (\gamma - 1) \ln(\rho/\rho_0) - s_0 T + \frac{p_\infty}{\rho},$$

where the parameters c_v , γ , p_∞ , T_0 , ρ_0 and s_0 are constants. From this we can derive the pressure law

$$(2.13) \quad p(\rho_i, e_i) = (\gamma_i - 1) \rho_i e_i - \gamma_i p_{\infty, i},$$

as well as the temperature law

$$(2.14) \quad c_{v, i} T = e_i - \frac{p_{\infty, i}}{\rho_i}$$

for each component i .

2.2 Quasilinear Formulation. In this section, we rewrite the system (2.2)–(2.4) in *quasilinear* form:

$$(2.15) \quad \frac{\partial \mathbf{U}}{\partial t} + \mathbf{A}(\mathbf{U}) \frac{\partial \mathbf{U}}{\partial x} = \mathbf{Q}(\mathbf{U}),$$

i.e. we obtain the matrix \mathbf{A} given by

$$(2.16) \quad \mathbf{A}(\mathbf{U}) = \frac{\partial \mathbf{F}(\mathbf{U})}{\partial \mathbf{U}}.$$

This will form the basis for the derivation of our Roe scheme in Section 3.2. The derivation is a generalization of the results of Abgrall [1], who considered a system of ideal gases with phase transition. However, whereas Abgrall's construction assumes that the pressure is given by Dalton's law, our Roe scheme allows for a general pressure function as described in Section 3.2.

First, we will find it convenient to split the flux vector into convective and pressure terms as follows:

$$(2.17) \quad \mathbf{F}(\mathbf{U}) = \mathbf{F}_c(\mathbf{U}) + \mathbf{F}_p(\mathbf{U}),$$

where

$$(2.18) \quad \mathbf{F}_c(\mathbf{U}) = v\mathbf{U}$$

and

$$(2.19) \quad \mathbf{F}_p(\mathbf{U}) = \begin{bmatrix} 0 \\ 0 \\ \vdots \\ 0 \\ p \\ pv \end{bmatrix}, \quad \mathbf{U} = \begin{bmatrix} m_1 \\ m_2 \\ \vdots \\ m_N \\ \rho v \\ E \end{bmatrix} = \begin{bmatrix} U_1 \\ U_2 \\ \vdots \\ U_N \\ U_{N+1} \\ U_{N+2} \end{bmatrix}.$$

Then we may write

$$(2.20) \quad \mathbf{A}(\mathbf{U}) = \mathbf{A}_c(\mathbf{U}) + \mathbf{A}_p(\mathbf{U}),$$

where

$$(2.21) \quad \mathbf{A}_c(\mathbf{U}) = \frac{\partial \mathbf{F}_c(\mathbf{U})}{\partial \mathbf{U}} \quad \text{and} \quad \mathbf{A}_p(\mathbf{U}) = \frac{\partial \mathbf{F}_p(\mathbf{U})}{\partial \mathbf{U}}.$$

PROPOSITION 1. *The convective Jacobian matrix $\mathbf{A}_c(\mathbf{U})$ can be written as*

$$(2.22) \quad \mathbf{A}_c = \begin{bmatrix} (1-Y_1)v & -Y_1v & \dots & -Y_1v & Y_1 & 0 \\ -Y_2v & (1-Y_2)v & \dots & -Y_2v & Y_2 & 0 \\ \vdots & \ddots & \ddots & \vdots & \vdots & \vdots \\ -Y_Nv & -Y_Nv & \dots & (1-Y_N)v & Y_N & 0 \\ -v^2 & -v^2 & \dots & -v^2 & 2v & 0 \\ -\mathcal{E}v & -\mathcal{E}v & \dots & -\mathcal{E}v & \mathcal{E} & v \end{bmatrix}$$

where

$$(2.23) \quad \mathcal{E} = \frac{E}{\rho}$$

and

$$(2.24) \quad Y_i = \frac{m_i}{\rho}.$$

Proof. From (2.18) we obtain

$$(2.25) \quad d\mathbf{F}_c = v d\mathbf{U} + \mathbf{U} dv,$$

which together with (2.5) and

$$(2.26) \quad dv = \frac{1}{\rho} (d(\rho v) - v d\rho)$$

yields the result.

PROPOSITION 2. *Define*

$$(2.27) \quad \mathcal{P}_i = \left(\frac{\partial p}{\partial m_i} \right)_{m_j \neq i, \epsilon} \quad i \in \{1, \dots, N\}$$

and

$$(2.28) \quad \mathcal{P}_\epsilon = \left(\frac{\partial p}{\partial \epsilon} \right)_{m_1, \dots, m_N}$$

so that (2.7) can be written in differential form as

$$(2.29) \quad dp = \mathcal{P}_\epsilon d\epsilon + \sum_{i=1}^N \mathcal{P}_i dm_i.$$

Then the pressure Jacobian matrix $\mathbf{A}_p(\mathbf{U})$ can be written as

$$(2.30) \quad \mathbf{A}_p^T = \begin{bmatrix} 0 & 0 & \dots & 0 & a_1 & v \left(a_1 - \frac{p}{\rho} \right) \\ 0 & 0 & \dots & 0 & a_2 & v \left(a_2 - \frac{p}{\rho} \right) \\ \vdots & \ddots & \ddots & \vdots & \vdots & \vdots \\ 0 & 0 & \dots & 0 & a_N & v \left(a_N - \frac{p}{\rho} \right) \\ 0 & 0 & \dots & 0 & -v\mathcal{P}_\epsilon & \frac{p}{\rho} - v^2\mathcal{P}_\epsilon \\ 0 & 0 & \dots & 0 & \mathcal{P}_\epsilon & v\mathcal{P}_\epsilon \end{bmatrix},$$

where

$$(2.31) \quad a_i = \mathcal{P}_i + \frac{1}{2}v^2\mathcal{P}_\epsilon \quad \forall i \in \{1, \dots, N\}.$$

Proof. From (2.6) and (2.26) we can derive the differential

$$(2.32) \quad dE = d\epsilon - \frac{1}{2}v^2 \sum_{i=1}^N dm_i + v d(\rho v),$$

by which we may rewrite (2.29) as

$$(2.33) \quad dp = \sum_{i=1}^N \left(\mathcal{P}_i + \frac{1}{2}v^2\mathcal{P}_\epsilon \right) dU_i - v\mathcal{P}_\epsilon dU_{N+1} + \mathcal{P}_\epsilon dU_{N+2}.$$

The result follows from (2.33) together with

$$(2.34) \quad d(pv) = p dv + v dp.$$

2.2.1 Eigenstructure. In this section, we analytically derive the eigenstructure of the matrix

$$(2.35) \quad \mathbf{A} = \begin{bmatrix} A_{11} & A_{12} & \dots & A_{1,N+2} \\ A_{21} & A_{22} & \dots & A_{2,N+2} \\ \vdots & \vdots & \ddots & \vdots \\ A_{N+2,1} & A_{N+2,2} & \dots & A_{N+2,N+2} \end{bmatrix}$$

given by (2.20), (2.22) and (2.30).

PROPOSITION 3. *The velocity v is an eigenvalue of the matrix \mathbf{A} , and the dimension \mathcal{D}_v of the corresponding eigenspace satisfies*

$$(2.36) \quad \mathcal{D}_v \geq N.$$

Proof. We look for eigenvectors satisfying

$$(2.37) \quad \mathbf{A}\boldsymbol{\omega} = v\boldsymbol{\omega},$$

where

$$(2.38) \quad \boldsymbol{\omega} = \begin{bmatrix} \omega_1 \\ \omega_2 \\ \vdots \\ \omega_N \\ \omega_{N+1} \\ \omega_{N+2} \end{bmatrix}.$$

Now observe that the equations

$$(2.39) \quad \sum_{j=1}^{N+2} A_{ij}\omega_j = v\omega_i$$

reduce to

$$(2.40) \quad \omega_{N+1} = v \sum_{j=1}^N \omega_j$$

for all $i \in \{1, \dots, N\}$ and

$$(2.41) \quad \sum_{i=1}^N \mathcal{P}_i \omega_i - \frac{1}{2} v \mathcal{P}_\epsilon \omega_{N+1} + \mathcal{P}_\epsilon \omega_{N+2} = 0$$

for $i \in \{N+1, N+2\}$. Hence there are at most 2 independent linear constraints on the elements of $\boldsymbol{\omega}$, and

$$(2.42) \quad \mathcal{D}_v \geq (N+2) - 2 = N.$$

PROPOSITION 4. *Assume that $\mathcal{P}_1, \dots, \mathcal{P}_N$ and \mathcal{P}_ϵ are all strictly positive. Then the eigenspace corresponding to the eigenvalue $\lambda = v$ is spanned by the basis vectors $\boldsymbol{\omega}^i$, where*

$$(2.43) \quad \boldsymbol{\omega}_j^i = \begin{cases} \mathcal{P}_N & \text{if } j = i, \\ -\mathcal{P}_i & \text{if } j = N, \\ v(\mathcal{P}_N - \mathcal{P}_i) & \text{if } j = N+1, \\ \frac{1}{2}v^2(\mathcal{P}_N - \mathcal{P}_i) & \text{if } j = N+2, \\ 0 & \text{otherwise} \end{cases}$$

for $i \in \{1, \dots, N-1\}$ and

$$(2.44) \quad \omega_j^N = \begin{cases} \mathcal{P}_\epsilon & \text{if } j = 1, \\ v\mathcal{P}_\epsilon & \text{if } j = N+1, \\ \frac{1}{2}v^2\mathcal{P}_\epsilon - \mathcal{P}_1 & \text{if } j = N+2, \\ 0 & \text{otherwise.} \end{cases}$$

Proof. Observe that when \mathcal{P}_ϵ is strictly positive, the constraints (2.40) and (2.41) are linearly independent, hence

$$(2.45) \quad \mathcal{D}_v = N.$$

Furthermore, note that the constraints (2.40)–(2.41) are satisfied, so (2.43) and (2.44) are in the eigenspace corresponding to $\lambda = v$.

Also, the $N-1$ vectors described by (2.43) are linearly independent since $\omega_j^j \neq 0$, $\omega_j^{i \neq j} = 0$ for all $j \in \{1, \dots, N\}$. Finally, (2.44) is linearly independent of the set (2.43), as all linear combinations of vectors in the form (2.43) satisfy

$$(2.46) \quad \forall i \in \{1, \dots, N-1\} \quad \sum_{j=1}^N \mathcal{P}_j \omega_j^i = 0,$$

which is not satisfied by (2.44).

In conclusion, the N vectors described by (2.43)–(2.44) are linearly independent and reside in the N -dimensional eigenspace corresponding to $\lambda = v$. Hence they form a basis for this space.

PROPOSITION 5. *The matrix \mathbf{A} has two eigenvalues given by*

$$(2.47) \quad \lambda = v \pm \tilde{c},$$

where

$$(2.48) \quad \tilde{c} = \sqrt{\sum_{i=1}^N Y_i \mathcal{P}_i + \frac{\epsilon + p}{\rho} \mathcal{P}_\epsilon}.$$

Proof. We look for eigenvectors satisfying

$$(2.49) \quad \mathbf{A}\boldsymbol{\omega} = (v+s)\boldsymbol{\omega},$$

where s is assumed to be non-zero. Now observe that the equations

$$(2.50) \quad \sum_{j=1}^{N+2} A_{ij}\omega_j = (v+s)\omega_i$$

may be simplified to yield the constraints

$$(2.51) \quad (v + s)\omega_j = Y_j\omega_{N+1} \quad \forall j \in \{1, \dots, N\},$$

$$(2.52)$$

$$(v + s)\mathcal{P}_\epsilon\omega_{N+2} = \left(s^2 - \sum_{i=1}^N \mathcal{P}_i Y_i + v \left(s + \frac{1}{2}v \right) \right) \omega_{N+1},$$

$$(2.53) \quad \left(\mathcal{P}_\epsilon \frac{\epsilon + p}{\rho} - s^2 + \sum_{i=1}^N \mathcal{P}_i Y_i \right) \omega_{N+1} = 0.$$

Furthermore, observe that (2.51)–(2.53) allow for non-trivial solutions if

$$(2.54) \quad s^2 = \sum_{i=1}^N \mathcal{P}_i Y_i + \frac{\epsilon + p}{\rho} \mathcal{P}_\epsilon,$$

or by (2.48):

$$(2.55) \quad s = \pm \tilde{c}.$$

PROPOSITION 6. *The eigenvectors corresponding to the eigenvalues $v \pm \tilde{c}$ can be expressed as*

$$(2.56) \quad \omega_j^\pm = \begin{cases} Y_j & \text{if } j \leq N \\ v \pm \tilde{c} & \text{if } j = N + 1 \\ \frac{\epsilon + p}{\rho} + \frac{1}{2}v^2 \pm v\tilde{c} & \text{if } j = N + 2. \end{cases}$$

Proof. The constraints (2.51)–(2.53) can be simplified by use of (2.55) to

$$(2.57) \quad (v \pm \tilde{c})\omega_j = Y_j\omega_{N+1},$$

$$(2.58) \quad (v \pm \tilde{c})\omega_{N+2} = \left(\frac{\epsilon + p}{\rho} + \frac{1}{2}v^2 \pm v\tilde{c} \right) \omega_{N+1},$$

which are satisfied by (2.56).

2.2.2 Primary variables. While the translation of the primary variables into the vector of conserved variables U is straightforward, the opposite direction is not. It involves the resolution of the system consisting of the definition of the conserved variables (U in equation (2.19)), two state equations per component (equations (2.13) and (2.14)) and the fact that the sum of the volume fractions is equal to one:

$$(2.59) \quad \sum_{i=1}^N \frac{U_i}{\rho_i} = 1.$$

First of all, the velocity is trivially found through

$$(2.60) \quad v = \frac{U_{N+1}}{\sum_{i=1}^N U_i}.$$

In order for the rest to be solved, it is reduced to a system of two equations. First, a relation between the

density of the component $i = 2, N$ and that of the component 1 is:

$$(2.61) \quad \rho_i = \frac{\frac{\gamma_i - 1}{\gamma_i} c_{p,1}}{\frac{\gamma_i - 1}{\gamma_i} c_{p,i}} \rho_1 - \frac{p_{\infty,1} - p_{\infty,i}}{\frac{\gamma_i - 1}{\gamma_i} c_{p,i} T}.$$

Then we can write

$$(2.62) \quad f_1 = \left(1 - \sum_{i=2}^N \frac{U_i}{\rho_i} \right) \rho_1 - U_1,$$

$$(2.63) \quad f_2 = \sum_{i=1}^N U_i \left(e_i + \frac{1}{2}v^2 \right) - U_{N+2}.$$

This system can be solved for ρ_1 and T using a Newton algorithm. The remaining variables follow from (2.61) and the equations of state.

3 Numerical Methods

A rough classification of finite volume methods for hyperbolic conservation laws separates between *central methods*, which are straightforward yet diffusive, and *upwind methods*, which are more accurate but can be algebraically cumbersome. A central-type method, the *MUSTA* scheme introduced by Toro [13], was employed in [9] for our current model.

The purpose of this paper is to adapt the Riemann solver of Roe [10] to our particular application. Roe's solver is a convenient upwind method, as it requires only the solution of a *linear* Riemann problem at each cell interface; see [10] for details.

For a related model, a Roe scheme has already been proposed by Abgrall [1], and we will closely follow his approach. The modification presented here allows us to construct a Roe scheme for *arbitrary* equations of state, as described in more detail in Section 3.2.2.

3.1 The Roe Method. Roe's method relies upon the construction of a matrix \hat{A} satisfying the following properties:

$$\text{R1: } \hat{A}(U^L, U^R)(U^R - U^L) = F(U^R) - F(U^L);$$

$$\text{R2: } \hat{A}(U^L, U^R) \text{ is diagonalizable with real eigenvalues;}$$

$$\text{R3: } \hat{A}(U^L, U^R) \rightarrow \frac{\partial F}{\partial U} \text{ smoothly as } U^L, U^R \rightarrow U.$$

We now consider a computational grid with space index j and time index n , such that

$$(3.64) \quad x_j = x_0 + j\Delta x$$

and

$$(3.65) \quad t^n = t_0 + n\Delta t.$$

The Roe scheme can now be written in *flux-conservative* form:

$$(3.66) \quad \frac{U_j^{n+1} - U_j^n}{\Delta t} + \frac{F_{j+1/2} - F_{j-1/2}}{\Delta x} = Q_j^n,$$

where the first-order numerical flux $F_{j+1/2}$ is given by

$$(3.67) \quad F_{j+1/2} = \frac{1}{2} (F(U_j^n) + F(U_{j+1}^n)) + |\hat{A}| (U_{j+1}^n - U_j^n)$$

where the “absolute value” of the matrix \hat{A} is given by

$$(3.68) \quad |\hat{A}| = \hat{R} |\hat{\Lambda}| \hat{R}^{-1},$$

with

$$(3.69) \quad |\hat{\Lambda}| = \text{diag}(|\lambda_1|, |\lambda_2|, \dots, |\lambda_{N+2}|),$$

where λ_i are the eigenvalues of \hat{A} , and \hat{R} is the matrix of eigenvectors that diagonalizes \hat{A} .

3.1.1 High Resolution. There are several ways of obtaining high resolution in the numerical solution. By “high resolution” we here mean second-order accuracy in smooth portions of the solution, and no spurious oscillations. In this work, we employ the method of characteristic flux-limiting described in LeVeque [7, Chapter 15] because of its accuracy and efficiency. Herein, the numerical scheme is formulated as

$$(3.70) \quad U_j^{n+1} = U_j^n - \frac{\Delta t}{\Delta x} \left(\mathcal{A}^- \Delta U_{j+1/2} + \mathcal{A}^+ \Delta U_{j-1/2} \right) - \frac{\Delta t}{\Delta x} \left(\tilde{F}_{j+1/2} - \tilde{F}_{j-1/2} \right),$$

where the symbol $\mathcal{A}^- \Delta U_{j+1/2}$ denotes the net effect of all left-going waves at $x_{j+1/2}$, and $\mathcal{A}^+ \Delta U_{j-1/2}$ measures the net effect of all right-going waves at $x_{j-1/2}$. The second-order correction $\tilde{F}_{j+1/2}$ is defined in the following.

For the Roe solver, we have the interpretation that

$$(3.71) \quad \mathcal{A}^\pm \Delta U_{j+1/2} = \hat{A}_{j+1/2}^\pm (U_{j+1} - U_j).$$

Herein,

$$(3.72) \quad \hat{A}_{j+1/2}^\pm = \hat{R}_{j+1/2} \hat{\Lambda}_{j+1/2}^\pm \hat{R}_{j+1/2}^{-1},$$

where $\hat{R}_{j+1/2}$ is the matrix having the right eigenvectors $\hat{r}_{j+1/2}$ of $\hat{A}_{j+1/2}$ as its columns, and $\hat{\Lambda}_{j+1/2}^+$ and $\hat{\Lambda}_{j+1/2}^-$ are the diagonal matrices containing the positive and negative eigenvalues, respectively, of $\hat{A}_{j+1/2}$. Further, to satisfy the condition R1, we must have that

$$(3.73) \quad \hat{A}_{j+1/2} (U_{j+1} - U_j) = \sum_{p=1}^{N+2} \lambda_{j+1/2}^p \mathcal{W}_{j+1/2}^p,$$

where $\mathcal{W}_{j+1/2}^p$ is the p th wave arising in the solution to the Riemann problem at $x_{j+1/2}$. The approximate Riemann solution consists of $N+2$ waves proportional to the right eigenvectors $\hat{r}_{j+1/2}$, propagating with speeds equal to the eigenvalues, $\lambda_{j+1/2}^p$, of $\hat{A}_{j+1/2}$. The proportionality coefficients $\beta_{j+1/2}^p$ can be found by solving the linear system

$$(3.74) \quad U_{j+1} - U_j = \sum_{p=1}^{N+2} \beta_{j+1/2}^p \hat{r}_{j+1/2}^p,$$

and $\beta_{j+1/2}^p$ can be interpreted as wave strengths.

The flux vector $\tilde{F}_{j+1/2}$ is the higher-order correction. It is given by

$$(3.75) \quad \tilde{F}_{j+1/2} = \frac{1}{2} \sum_{p=1}^{N+2} |\lambda_{j+1/2}^p| \left(1 - \frac{\Delta t}{\Delta x} |\lambda_{j+1/2}^p| \right) \widetilde{\mathcal{W}}_{j+1/2}^p,$$

where $\widetilde{\mathcal{W}}_{j+1/2}^p$ is a limited version of the wave $\mathcal{W}_{j+1/2}^p$. The limited waves $\widetilde{\mathcal{W}}_{j+1/2}^p$ are found by comparing the wave $\mathcal{W}_{j+1/2}^p$ with the upwind wave $\mathcal{W}_{J+1/2}^p$ [7, see Section 9.13], where

$$(3.76) \quad J = \begin{cases} j-1 & \text{if } \lambda_{j+1/2}^p \geq 0, \\ j+1 & \text{if } \lambda_{j+1/2}^p < 0. \end{cases}$$

We write

$$(3.77) \quad \widetilde{\mathcal{W}}_{j+1/2}^p = \phi(\theta_{j+1/2}^p) \mathcal{W}_{j+1/2}^p,$$

where ϕ is a flux-limiter function, and $\theta_{j+1/2}^p$ is a measure of the smoothness of the p th characteristic component of the solution:

$$(3.78) \quad \theta_{j+1/2}^p = \frac{\mathcal{W}_{J+1/2}^p \cdot \mathcal{W}_{j+1/2}^p}{\mathcal{W}_{j+1/2}^p \cdot \mathcal{W}_{j+1/2}^p},$$

where \cdot denotes the scalar product in \mathbb{R}^{N+2} .

In Section 4, we will employ the minmod limiter, see [11],

$$(3.79) \quad \phi(\theta) = \text{minmod}(1, \theta),$$

where

$$(3.80) \quad \text{minmod}(a, b) = \begin{cases} 0 & \text{if } ab \leq 0, \\ a & \text{if } |a| < |b| \text{ and } ab > 0, \\ b & \text{if } |a| \geq |b| \text{ and } ab > 0, \end{cases}$$

the monotized central-difference (MC) limiter [14],

$$(3.81) \quad \phi(\theta) = \max(0, \min((1 + \theta)/2, 2, 2\theta)),$$

and the superbee limiter [11],

$$(3.82) \quad \phi(\theta) = \max(0, \min(1, 2\theta), \min(2, \theta)),$$

(see also [7, Section 6.11]).

3.2 A Semi-Analytical Roe Matrix. In this section, we construct a Roe matrix in the so-called *quasi-Jacobian* form [4], following closely the approach of Abgrall [1]. We will take advantage of the flux splitting (2.17), and write the Roe matrix as

$$(3.83) \quad \hat{\mathbf{A}} = \hat{\mathbf{A}}_c + \hat{\mathbf{A}}_p.$$

PROPOSITION 7. *The convective Roe matrix given by*

$$(3.84) \quad \hat{\mathbf{A}}_c = \begin{bmatrix} (1 - \hat{Y}_1)\hat{v} & -\hat{Y}_1\hat{v} & \dots & -\hat{Y}_1\hat{v} & \hat{Y}_1 & 0 \\ -\hat{Y}_2\hat{v} & (1 - \hat{Y}_2)\hat{v} & \dots & -\hat{Y}_2\hat{v} & \hat{Y}_2 & 0 \\ \vdots & \ddots & \ddots & \vdots & \vdots & \vdots \\ -\hat{Y}_N\hat{v} & -\hat{Y}_N\hat{v} & \dots & (1 - \hat{Y}_N)\hat{v} & \hat{Y}_N & 0 \\ -\hat{v}^2 & -\hat{v}^2 & \dots & -\hat{v}^2 & 2\hat{v} & 0 \\ -\hat{\mathcal{E}}\hat{v} & -\hat{\mathcal{E}}\hat{v} & \dots & -\hat{\mathcal{E}}\hat{v} & \hat{\mathcal{E}} & \hat{v} \end{bmatrix}$$

where

$$(3.85) \quad \hat{Y}_i = \frac{\sqrt{\rho_j}Y_{i,j} + \sqrt{\rho_{j+1}}Y_{i,j+1}}{\sqrt{\rho_j} + \sqrt{\rho_{j+1}}},$$

$$(3.86) \quad \hat{v} = \frac{\sqrt{\rho_j}v_j + \sqrt{\rho_{j+1}}v_{j+1}}{\sqrt{\rho_j} + \sqrt{\rho_{j+1}}},$$

$$(3.87) \quad \hat{\mathcal{E}} = \frac{\sqrt{\rho_j}\hat{\mathcal{E}}_j + \sqrt{\rho_{j+1}}\hat{\mathcal{E}}_{j+1}}{\sqrt{\rho_j} + \sqrt{\rho_{j+1}}},$$

satisfies the Roe condition

$$(3.88) \quad \hat{\mathbf{A}}_{c,j+1/2}(\mathbf{U}_{j+1} - \mathbf{U}_j) = \mathbf{F}_c(\mathbf{U}_{j+1}) - \mathbf{F}_c(\mathbf{U}_j).$$

Proof. As described in [1, 3], this result can be derived using Roe's approach [10] with the parameter vector:

$$(3.89) \quad \mathbf{q} = \sqrt{\rho} \begin{bmatrix} Y_1 \\ \vdots \\ Y_N \\ v \\ \hat{\mathcal{E}} \end{bmatrix}.$$

3.2.1 The Pressure Roe Matrix. We write the Roe matrix $\hat{\mathbf{A}}_p$ as

$$(3.90) \quad \hat{\mathbf{A}}_p^T = \begin{bmatrix} 0 & 0 & \dots & 0 & \hat{a}_1 & \hat{v} \left(\hat{a}_1 - \widehat{\left[\frac{p}{\rho} \right]} \right) \\ 0 & 0 & \dots & 0 & \hat{a}_2 & \hat{v} \left(\hat{a}_2 - \widehat{\left[\frac{p}{\rho} \right]} \right) \\ \vdots & \ddots & \ddots & \vdots & \vdots & \vdots \\ 0 & 0 & \dots & 0 & \hat{a}_N & \hat{v} \left(\hat{a}_N - \widehat{\left[\frac{p}{\rho} \right]} \right) \\ 0 & 0 & \dots & 0 & -\hat{v}\hat{\mathcal{P}}_\epsilon & \widehat{\left[\frac{p}{\rho} \right]} - \hat{v}^2\hat{\mathcal{P}}_\epsilon \\ 0 & 0 & \dots & 0 & \hat{\mathcal{P}}_\epsilon & \hat{v}\hat{\mathcal{P}}_\epsilon \end{bmatrix},$$

where

$$(3.91) \quad \hat{a}_i = \hat{\mathcal{P}}_i + \frac{1}{2}\hat{v}^2\hat{\mathcal{P}}_\epsilon \quad \forall i \in \{1, \dots, N\}.$$

PROPOSITION 8. *The pressure Roe matrix given by (3.90) satisfies the Roe condition*

$$(3.92) \quad \hat{\mathbf{A}}_{p,j+1/2}(\mathbf{U}_{j+1} - \mathbf{U}_j) = \mathbf{F}_p(\mathbf{U}_{j+1}) - \mathbf{F}_p(\mathbf{U}_j),$$

provided that \hat{v} is given by (3.86), and

$$(3.93) \quad \widehat{\left[\frac{p}{\rho} \right]} = \frac{\sqrt{\rho_{j+1}}p_j + \sqrt{\rho_j}p_{j+1}}{\sqrt{\rho_{j+1}}\rho_j + \sqrt{\rho_j}\rho_{j+1}},$$

and the subcondition

$$(3.94) \quad \hat{\mathcal{P}}_\epsilon(\epsilon_{j+1} - \epsilon_j) + \sum_{i=1}^N \hat{\mathcal{P}}_i(m_{i,j+1} - m_{i,j}) = p_{j+1} - p_j$$

is satisfied.

Proof. The result may be verified by substituting (2.19) and (3.90) with (3.86), (3.93) and (3.94) into (3.92).

3.2.2 The Roe-Averaged Pressure Derivative.

We have now reduced the problem to finding a suitable Roe-type average of the form (3.94) for the pressure function $p(\epsilon, m_1, \dots, m_N)$. In general, these averages can be calculated analytically for any given case of an analytical pressure function $p(\epsilon, m_1, \dots, m_N)$.

However, as the purpose of this paper is to keep the method as general as possible, we will use an approach similar in spirit to the suggestion of Glaister [6]. In particular, our approach here is identical to the one used in [5] for a different model.

Following [5], we first introduce the symbol $\Delta_{(r)}$ given by

$$(3.95) \quad \Delta_{(r)}p(\mathbf{q}^L, \mathbf{q}^R) = p(q_1^R, \dots, q_r^R, q_{r+1}^L, \dots, q_M^L) - p(q_1^R, \dots, q_{r-1}^R, q_r^L, \dots, q_M^L),$$

where the $(M = N + 1)$ -vector \mathbf{q} is given by

$$(3.96) \quad \mathbf{q} = \begin{bmatrix} m_1 \\ \vdots \\ m_N \\ \epsilon \end{bmatrix}.$$

We then have that

$$(3.97) \quad \hat{\mathcal{P}}_r = \begin{cases} \frac{\Delta_{(r)}p(\mathbf{q}^L, \mathbf{q}^R)}{q_r^R - q_r^L} & \text{for } q_r^L \neq q_r^R \\ \frac{\partial p}{\partial q_r}(\mathbf{q}^R) & \text{otherwise} \end{cases}$$

satisfies the condition (3.94) for all functions $p(m_1, \dots, m_N, \epsilon)$. Furthermore, the Roe condition

Table 1: EOS parameters employed in the present calculations.

	γ_i (-)	$p_{\infty,i}$ (MPa)	$c_{p,i}$ (kJ/(kg K))
carbon dioxide (1)	1.03	13.47	3.877
water (2)	2.85	833.02	4.155
methane (3)	1.23	10.94	2.930

Table 2: Initial state in the moving-discontinuity problem.

Quantity	Symbol (unit)	Left	Right
CO ₂ vol. frac.	α_1 (-)	0.8	0.2
Water vol. frac.	α_2 (-)	0.2	0.8
Velocity	v (m/s)	10	10
Pressure	p (MPa)	10	10
Temperature	T (K)	310	310

R3 is also satisfied; see [5] for details. The condition R2 is satisfied provided the sound velocity \tilde{c} is real, or equivalently that s as given by (2.54) satisfies

$$(3.98) \quad s^2 \geq 0.$$

Note in particular that this is the case if $\hat{P}_1, \dots, \hat{P}_N$ and \hat{P}_e are all strictly positive. This assumption is also made in Proposition 4.

4 Numerical Simulations

In this section, the Roe scheme is tested with respect to stability, accuracy and robustness. Further, it is compared to an independent scheme, namely the MUSTA scheme described by Munkejord *et al.* [9].

The equation-of-state parameters have been adapted to carbon dioxide (component 1), water (component 2) and methane (component 3) at 10 MPa and 310 K, and are shown in Table 1.

4.1 Moving discontinuity. We consider a case which tests how the numerical method captures a moving discontinuity. Initially, all variables are uniform, except for a discontinuity in the volume fraction in the middle of the tube, see Table 2. Ideally, the numerical method should advect the volume-fraction discontinuity without smearing it.

Calculations have been performed with the Roe scheme and the two-stage two-cell MUSTA scheme using a CFL number of $r = 0.9$ on various grids. Figure 1 shows the CO₂ volume fraction at $t = 1.5$ s. Both numerical schemes behave well, without introducing spurious oscillations. However, the MUSTA scheme is

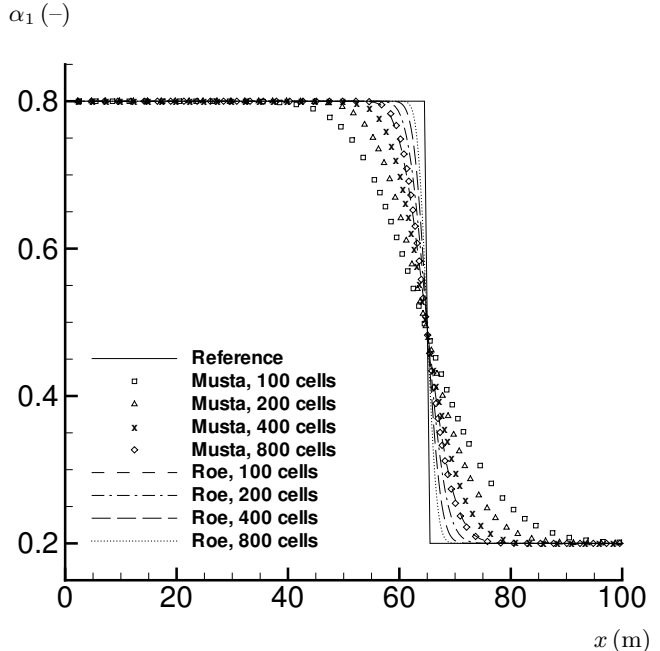


Figure 1: Moving-discontinuity problem. CO₂ volume fraction for the MUSTA and Roe schemes. $r = 0.9$.

Table 3: Initial state in the shock-tube problem.

Quantity	Symbol (unit)	Left	Right
CO ₂ vol. frac.	α_1 (-)	0.9	0.9
Water vol. frac.	α_2 (-)	0.04	0.04
Methane vol. frac.	α_3 (-)	0.06	0.06
Velocity	v (m/s)	0	0
Pressure	p (MPa)	1.5	0.9
Temperature	T (K)	310	310

more dissipative than the Roe scheme. In this case, the MUSTA scheme gives roughly the same solution on an 800-cell grid as that produced with the Roe scheme on a 100-cell grid.

4.2 Shock Tube. The present test case is a Riemann problem set up to investigate basic consistency properties of the Roe scheme. The physical interpretation is a tube divided by a membrane in the middle. At $t = 0$, the membrane ruptures, and the flow starts evolving. The initial conditions are given in Table 3.

Calculations have been performed on various grids using a CFL number of $r = 0.9$. Figures 2–3 display the physical variables at $t = 0.1$ s. The reference solution has been obtained using the two-stage two-cell MUSTA scheme on a fine grid of 20 000 cells. The figures show that the solution calculated using the Roe

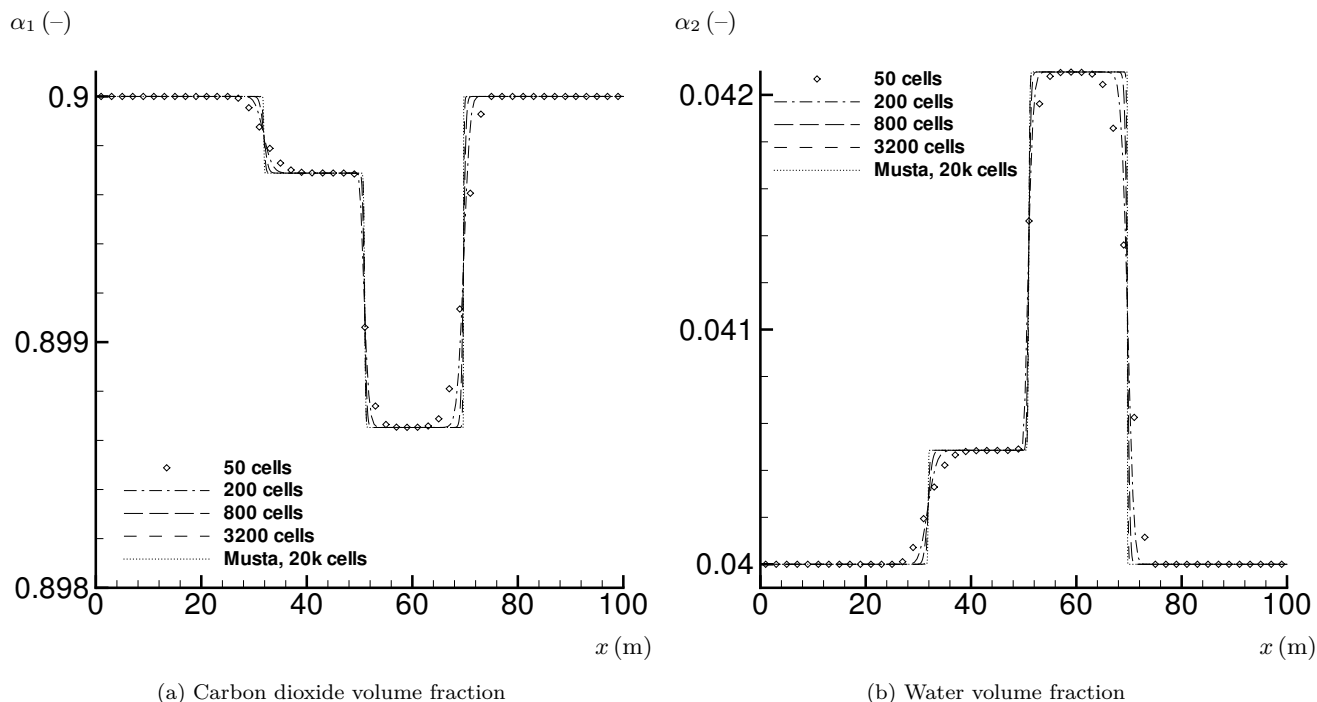


Figure 2: Shock-tube problem. Convergence of the Roe scheme, $r = 0.9$. Volume fractions.

scheme converges towards the reference solution without oscillations.

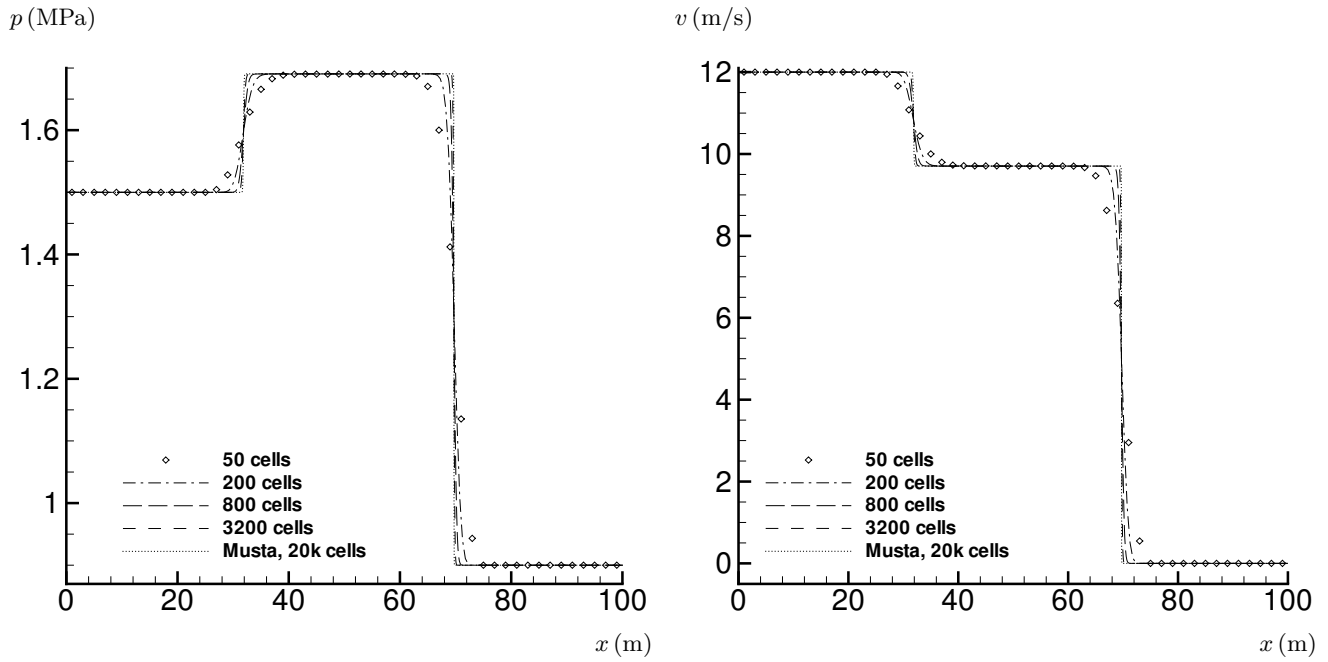
4.3 Depressurization Case. This test case is an example of a possible industrial application. It simulates the instantaneous depressurization of a tube at its right end, followed by a repressurization at the previous pressure. This creates a low-pressure wave propagating to the left. In this case where only liquids are involved, this is accompanied by a slight temperature decrease. However, things change for a system where phase change is allowed, which finds direct application in industry. The low-pressure wave would lead to an evaporation, and thus to a strong cooling. This cooling is of interest when one wishes to evaluate the mechanical properties of a metal pipe, for example. As the cooling is sensitive to the amplitude of the pressure wave, it becomes critically important to numerically reproduce such waves correctly.

The case consists of a 1000 m long pipe filled with an initially motionless mixture at 10 MPa and 300 K. The mixture is composed of carbon dioxide, water and methane with initial volume fractions respectively being 0.9, 0.09 and 0.01. The component properties used are shown in Table 1. At $t = 0$ s, the pressure is instantaneously decreased to 1 MPa, and set back to 10 MPa at $t = 2$ s. The boundary conditions used are

designed to respect the information propagation. This model includes five conservation equations, therefore five independent quantities are advected in waves. Two of those are mass fractions waves, one is the mixture entropy wave and two are sound waves. Depending on their propagation direction, they will either be created or disappear at the boundary. In this case, where the velocity is always positive or zero, four of the waves leave the domain at the right; the last one - the left-going sound wave - enters it. Consequently, the last cell at the right of the domain is copied into a ghost boundary cell. The required pressure is then set in this boundary cell at constant mass fractions and mixture entropy.

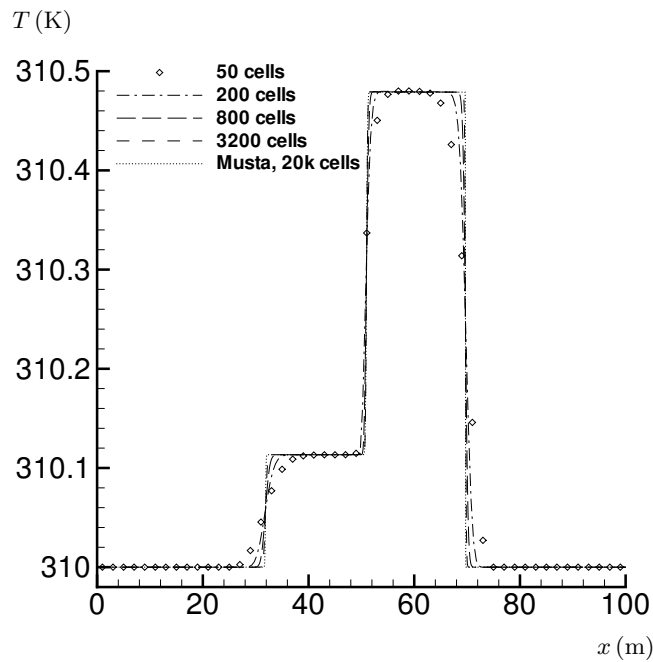
Figures 4–5 show the result of calculations that have been performed on a grid of 100 cells, except the reference solution which uses 1000 cells. The pressure is recorded at a position of 450 m from the right, over 6.5 s.

Several methods have been compared to evaluate their ability to preserve the amplitude of the low-pressure wave. Figure 4 shows the results for the MUSTA method and the Roe method without limiters, which are both first order. The three curves are almost superimposed and a significant smoothing of the pressure wave can be seen. The Roe method is then made second order by adding flux limiters.



(a) Pressure

(b) Velocity



(c) Temperature

Figure 3: Shock-tube problem. Convergence of the Roe scheme, $r = 0.9$. Pressure, velocity and temperature.

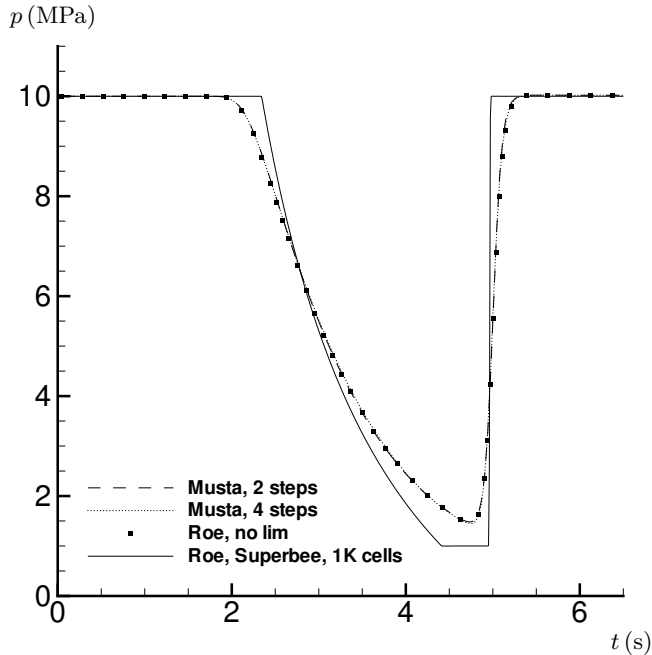
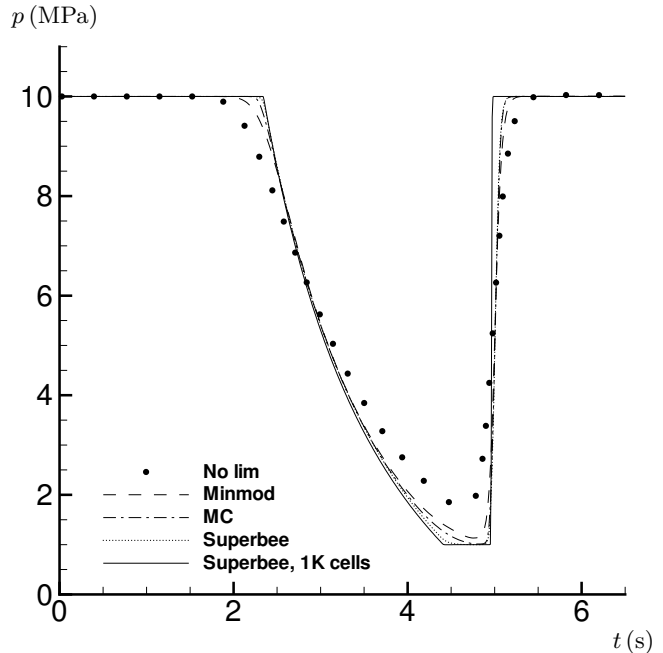


Figure 4: Depressurization case. Pressure as a function of time at $x = 450$ m. Comparison of the first-order Musta and Roe methods. 100 cells, $r = 0.9$.



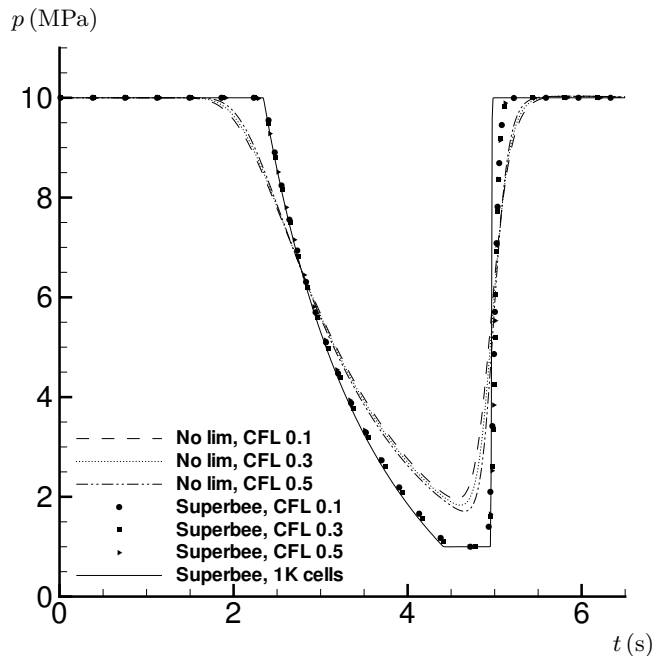
(a) Different flux limiters, $r = 0.5$.

In Figure 5(a), the results for three different flux limiters (minmod, monotonized central-difference (MC) and superbee) are compared to the version without limiters (No lim). MC performs quite well, but the best in this case is superbee. Here, the shape of the pressure wave is well conserved. Finally, the influence of the CFL number, r , deserves discussion. It may have a significant effect on the numerical viscosity. Since only a global limit can be imposed, the actual local CFL number can be very different along the computational domain. Therefore, methods maintaining accuracy for low CFL numbers are needed. Figure 5(b) shows that the flux limiters added to the Roe scheme, here superbee, make it basically insensitive to the CFL number, while the first-order scheme becomes more diffusive as the CFL number decreases.

Additionally, a grid refinement test has been performed on the Roe method with superbee limiter (Figure 6). It shows that already with 100 cells, the shock resolution is quite sharp.

5 Summary

We have presented a formulation of the approximate Riemann solver of Roe for a multicomponent flow model, allowing for a general formulation of the thermodynamic closure relations. We have incorporated high resolution (second order accuracy for smooth solutions)



(b) Effect of varying CFL number with and without flux limiters.

Figure 5: Depressurization case. Pressure as a function of time at $x = 450$ m. Roe method, 100 cells.

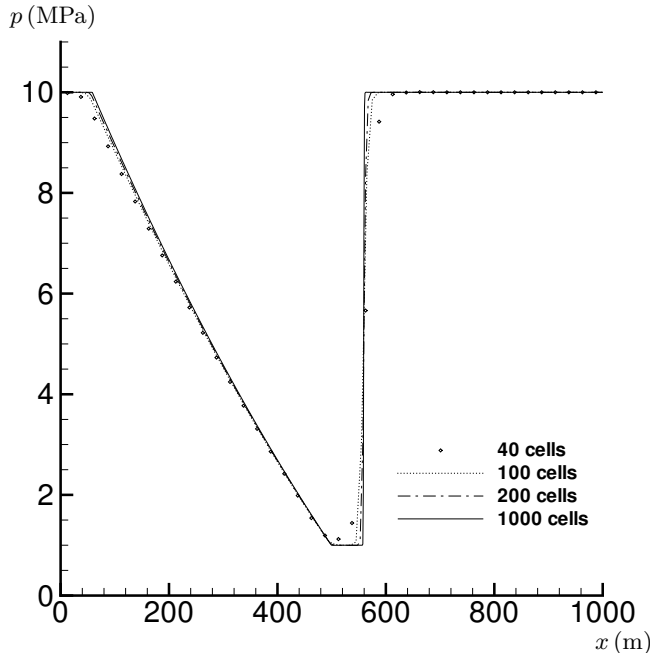


Figure 6: Depressurization case. Pressure as a function of position at $t = 4.9$ s. Grid refinement for the Roe method with superbee limiter, $r = 0.5$.

by means of the *wave limiter* approach. Our solver is relatively efficient, as an analytical formulation of its eigenstructure is available.

By numerical simulations, we have compared our solver to a more straightforward first-order central scheme. The results clearly show that numerical dissipation, which introduces a significant amount of error for the first-order scheme, may be satisfactorily controlled with our high-resolution Roe solver.

In particular, we have presented a case representing the effect of depressurization of a pipe relevant for the industry. Using a computational grid that would be representative for industrial simulations, we have seen that the central scheme underestimates the maximum amplitude of a pressure pulse by as much as 9.5 percent, whereas the high-resolution Roe scheme is able to capture the pulse with a high degree of accuracy.

Hence, we conclude that a proper choice of a numerical method plays an integral part in industrial operations analysis and simulation.

Acknowledgements

The first author has received a PhD grant from the BIGCCS Centre [2] and the work of the remaining authors was financed through the CO₂ Dynamics project. The authors acknowledge the support from the Research Council of Norway, Aker Solutions, ConocoPhillips

Skandinavia AS, Det Norske Veritas AS, Gassco AS, Hydro Aluminium AS, Shell Technology AS, Statkraft Development AS, StatoilHydro Petroleum AS, TOTAL E&P Norge AS and Vattenfall Research and Development AB.

References

- [1] R. Abgrall, *An extension of Roe's upwind scheme to algebraic equilibrium real gas models*, *Comput. Fluids* 19 (1991), pp. 171–182.
- [2] BIGCCS, *International CCS Research Centre*, <http://www.sintef.no/Projectweb/BIGCCS/>
- [3] D. Chargy, R. Abgrall, L. Fezoui and B. Larroutour, *Comparisons of several upwind schemes for multi-component one-dimensional inviscid flows*, *Rapports de Recherche N° 1253*, INRIA, France, 1990.
- [4] P. Cinnella, *Roe-type schemes for dense gas flow computations*, *Comput. Fluids* 35 (2006), pp. 1264–1281.
- [5] T. Flåtten and S. T. Munkejord, *The approximate Riemann solver of Roe applied to a drift-flux two-phase flow model*, *ESAIM-Math. Model. Num.*, 40 (2006), pp. 735–764.
- [6] P. Glaister, *An approximate linearized Riemann solver for the Euler equations for real gases*, *J. Comput. Phys.* 74 (1988), pp. 382–408.
- [7] R. J. LeVeque, *Finite Volume Methods for Hyperbolic Problems*, Cambridge University Press, Cambridge, UK, 2002.
- [8] R. Menikoff, *Empirical EOS for solids*, in *Shock Wave Science and Technology Reference Library, Volume 2 - Solids I*, Springer Berlin Heidelberg New York, 2007, pp. 143–188.
- [9] S. T. Munkejord, J. P. Jakobsen, A. Austegard and M. J. Mølnvik, *Thermo- and fluid-dynamical modeling of two-phase multi-component carbon dioxide mixtures*, *Energy Procedia*, 1 (2009), pp. 1649–1656.
- [10] P. L. Roe, *Approximate Riemann solvers, parameter vectors, and difference schemes*, *J. Comput. Phys.*, 43 (1981), pp. 357–372.
- [11] P. L. Roe, *Some contributions to the modeling of discontinuous flows*, *Lect. Appl. Math.*, 22 (1985), pp. 163–193.
- [12] J. E. Romate, *An approximate Riemann solver for a two-phase flow model with numerically given slip relation*, *Comput. Fluids*, 27 (1998), pp. 455–477.
- [13] E. F. Toro, *MUSTA: A multi-stage numerical flux*, *Appl. Numer. Math.*, 56 (2006), pp. 1464–1479.
- [14] B. van Leer, *Towards the ultimate conservative difference scheme IV. New approach to numerical convection*, *J. Comput. Phys.*, 23 (1977), pp. 276–299.